ADVANCED MATERIALS INTERFACES
Open Access
www.advmatinterfaces.de

Tuning Transition Metal-Containing Molecular Magnets by On-Surface Polymerization

Daniel Baranowski, Iulia Cojocariu, Luca Schio, Carolina Gutiérrez Bolaños, Luca Floreano, Jan Dreiser, Silvia Carlotto, Maurizio Casarin, Vitaliy Feyer,* and Claus Michael Schneider*

Porphyrins are promising multifunctional units particularly interesting for the realization of molecular nanodevices. Their structural variety allows to create precursors suitable for the on-surface polymerization of porphyrin blocks. The corresponding increased stability and improved transport properties of the formed polymerized molecular nanostructures make them practically worthwhile. For the case of 2D porphyrin materials, the effect of polymerization on the magnetic properties of transition metal ions has not been reported yet. Therefore, details on the properties of an extended covalent nickel tetraphenylporphyrin network formed via Ullmann coupling on the Cu(111) surface are reported. By using photoelectron and absorption spectroscopies together with density functional theory calculations, it is systematically evolving how the functional properties of the Ni centers are changed within a polymerized molecular structure in comparison to single-molecule nickel tetraphenylporphyrin derivatives that build the 2D molecular network. A model that explains the differences in the electronic and magnetic properties observed for the Ni centers in both structures based on the additional rigidity characteristic of the molecular layer after polymerization is drawn.

1. Introduction

Porphyrin molecules offer the unique opportunity to build nanoarchitectures at well-defined interfaces, where a variety of functional transition metal ions stabilized within the molecular moiety can be combined with diverse molecular substitutions that allow controllable chemical and optoelectronic properties.[1,2] The supporting interface further introduces the possibility of catalyzing confined reactions that alter the molecular conformation, e.g., thermally-activated porphyrin dehydrogenation, and turn out to influence the chemical reactivity and magnetic properties of porphyrin molecules.[3–5] In this regard molecular devices supported at well-defined interfaces attainable by covalent on-surface confined polymerization may further benefit from the improvement

D. Baranowski, I. Cojocariu, V. Feyer, C. M. Schneider
Peter Grünberg Institute (PGI-6)
Jülich Research Center
52428 Jülich, Germany
E-mail: d.baranowski@fz-juelich.de; v.feyer@fz-juelich.de

I. Cojocariu
Dipartimento di Fisica
Università degli Studi di Trieste
Trieste 34127, Italy

I. Cojocariu, C. G. Bolaños
Elettra-Sincrotrone S.C.p.A
Trieste 34149, Italy

L. Schio, L. Floreano
TASC Laboratory
CNR-IOM
Trieste 34149, Italy

The ORCID identification number(s) for the author(s) of this article can be found under https://doi.org/10.1002/admi.202400123

DOI: 10.1002/admi.202400123

C. G. Bolaños, J. Dreiser
Photon Science Division
Paul Scherrer Institute (PSI)
Villigen 5232, Switzerland

S. Carlotto
Department of Chemical Sciences
University of Padova
Padova 35131, Italy

S. Carlotto, M. Casarin
Institute of Condensed Matter Chemistry and Technologies for Energy (ICMATE)
CNR c/o Department of Chemical Sciences
University of Padova
Padova 35131, Italy

V. Feyer, C. M. Schneider
Faculty of Physics and Center for Nanointegration Duisburg-Essen (CENIDE)
University of Duisburg-Essen
47048 Duisburg, Germany

C. M. Schneider
Department of Physics, Astronomy
University of California Davis
Davis, CA 95616, USA

of their stability and optoelectronic properties.[6,7] It was further demonstrated that the single ion configuration is uniform across covalently extended porphyrin structures.[8] For extended one-dimensional metalloporphyrin chains, it was shown that the magnetic anisotropy can be manipulated by cyclo-dehydrogenation without any differences between the functional centers stabilized within the polymerized structure and those of their single-molecule counterparts.[9] However, it remains largely unexplored how the magnetic properties of the central metal ion are influenced within 2D nanostructures as a consequence of the polymerization of the molecular constituents and the formation of a π-extended molecular backbone. With the opportunity to tune the electronic properties of the molecular nanosheet by charge transfer at the interface, a prototype system with only one unpaired electron can be addressed. The present work addresses the peculiarities of the formation of a covalent network built from nickel tetraphenylporphyrin (NiTPP) units obtained through the Ullmann coupling reaction at the Cu(111) surface. This metal-catalyzed polymerization reaction, based on the homolytic cleavage of C—Br bonds before intermolecular C—C bond formation, is known from solution chemistry and emerged as a prominent covalent coupling scheme on coinage metals.[10] Utilizing the nickel tetra(4-bromophenyl)porphyrin (NiTBrPP) precursor, which exhibits both chemical stability and mobility on metal surfaces,[7] efficient intermolecular coupling was realized. Upon thermally-induced polymerization accompanied by dehydrogenation reactions of the activated NiTBrPP units, the pristine phenyl substituents are forced into a geometric configuration closely parallel to the surface. Such a planarity increases the molecule-substrate interaction and results in a Ni(II) to Ni(I) reduction of the Ni ion centers in the NiTPP-based network. The corresponding molecular nanosheet is a prototype system since the charge transfer at the interface offers the opportunity of addressing the electron properties of a system with only one unpaired electron. As the anisotropic magnetic properties are driven by the energy level alignment of the Ni 3d-based molecular orbitals (MOs) without additional complications arising from zero-field splitting, a systematic characterization approach is possible. Indeed, the monomeric units within this covalent nanomesh are chemically related to single-molecule NiTPP units that are flattened by cyclo-dehydrogenation (dh-NiTPP). When comparing the molecular constituents of the covalent NiTPP-based network with their single-molecule counterparts, it becomes evident that their magnetic response as well as their orbital magnetic moment anisotropy are drastically influenced as a consequence of on-surface polymerization. The findings presented here were obtained by combining X-ray photoelectron spectroscopy (XPS), near-edge X-ray absorption fine structure (NEXAFS) as well as X-ray magnetic circular dichroism (XMCD) and were further supported by density functional theory (DFT) calculations.

2. Results and Discussion

Different initial NiTBrPP coverages below one monolayer (ML) were used as a starting point for the surface-assisted Ullmann coupling on the Cu(111) surface. A sketch of the relevant functionalities of the molecular precursor is displayed in **Figure 1**. The C—Br bonds, which are highlighted by the violet dashed line, can be cleaved by catalytically active surfaces and are predefined points for the creation of new intermolecular C—C bonds induced by annealing.[6,7] Porphyrins with phenyl substituents are flexible upon stabilization on surfaces, which can result in tilted and twisted phenyl configurations as indicated by the blue arrows in Figure 1.[11,12] Intramolecular C—C coupling, resulting from cyclo-dehydrogenation involving flexible phenyl substituents, is further relevant when annealing porphyrin layers to elevated temperatures.[13] An example of a possible C—C linking between the porphyrin's macrocycle and a phenyl group is indicated by the orange arrow in Figure 1.

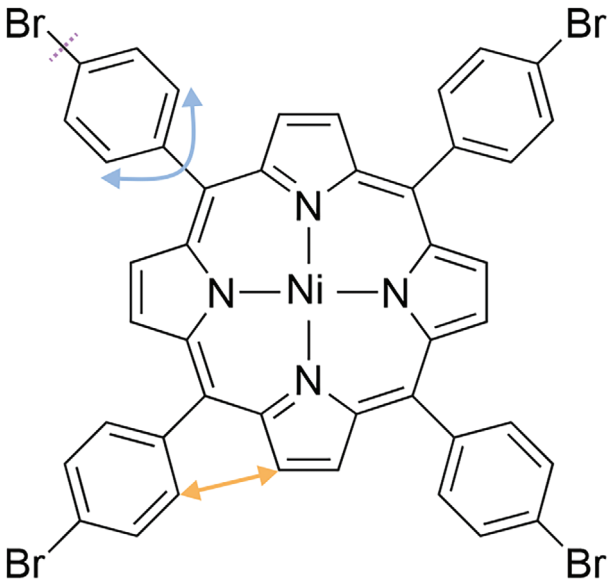

Figure 1. Sketch of the NiTBrPP ($C_{44}H_{24}N_4Br_4Ni$) precursor used for Ullmann coupling on Cu(111).

The Cu 3p and Br 3d photoelectron lines of the respective pristine NiTBrPP layers at different coverages are depicted in **Figure 2**. All spectra were normalized to the intensity of the Cu 3p signal. In both cases, the Br 3d signal indicates the exclusive presence of a single species with the main line at a binding energy (BE) of 68.6 eV. Since the observed BE corresponds to Br chemisorbed to Cu after C—Br bond cleavage,[14–16] it can be concluded that NiTBrPP molecules are readily activated when deposited on the surface kept at room temperature. The respective precursor layers, which consist of Ni porphyrin radicals, were then annealed to 473 K to induce covalent linking of the activated molecular units while avoiding the decomposition of the molecular layer.[17] The XPS spectra acquired after this thermal treatment are also included in Figure 2. Chemisorbed Br is not removed from the substrate when inducing Ullmann coupling of the molecular units, as is apparent from the Br 3d signal that remained constant after annealing for both initial coverages. Figure 2 further includes the corresponding normalized Ni $2p_{3/2}$ XPS spectra for the different initial coverages before and after annealing. The BE characteristic of the Ni centers stabilized within the porphyrin moiety is shifted from 855.6 to 853.2 eV after inducing Ullmann coupling.

This variation indicates the Ni(II) to Ni(I) reduction upon the polymerization of the molecular units as further elaborated in the following.[18] Only for an initial coverage of 0.7 ML, or below, the

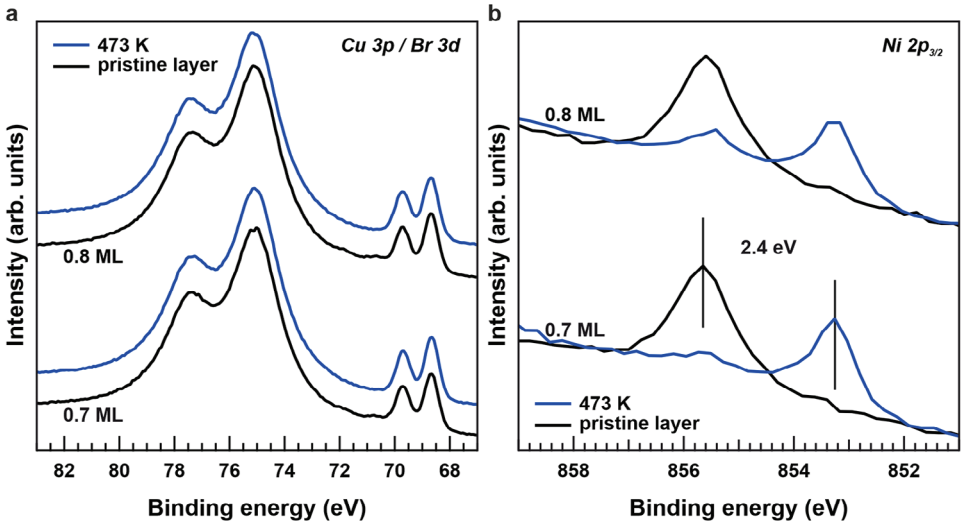

Figure 2. a) Cu 3p/Br 3d and b) Ni $2p_{3/2}$ XPS spectra collected for different coverages of as-deposited NiTBrPP on Cu(111) and after subsequent annealing to 473 K.

Ni centers are fully converted from their pristine configuration, while a remaining Ni(II) component is appreciable for pristine layers exceeding 0.8 ML. Ullmann coupling on Cu(111) is known to occur through an activated C—Cu—C complex.[19] The reaction confined to an interface free to react requires a catalytic surface that is not poisoned nor inducing steric hindrance by a too high amount of chemisorbed Br that is linearly increasing with the coverage of the brominated monomer.[20] We experimentally observe that this limits the coverage to a maximum of 0.7 ML NiTBrPP for a complete polymerization at the interface. Therefore, we never exceeded this coverage to avoid the presence of unconverted units.

Cu(111) is a highly reactive surface and it is, thus, surprising that the functional centers of the pristine molecular layer are in the Ni(II) state and are only reduced after inducing Ullmann coupling.[21] To better understand this behavior, we characterized the chemical changes after annealing 0.7 ML of the pristine molecular layer to 473 K by NEXAFS. The respective spectra recorded across both the C and N K-edges are depicted in **Figure 3**. NEXAFS is a highly efficient tool to determine the average on-surface orientation of adsorbed molecules. The intensities of the transitions from center levels into antibonding levels probed with the light polarization either parallel (p-polarization) or orthogonal (s-polarization) to the surface normal are different for oriented molecules, which is referred to as linear dichroism.[22] Indeed, the transitions monitored across the C K-edge for porphyrins correspond to 1s transitions into π^*-symmetry MOs and can be separated into macrocycle-based (index m) and phenyl-based MOs (index p).[23–27] The C K-edge spectra recorded using p- and s-polarized light display a poor linear

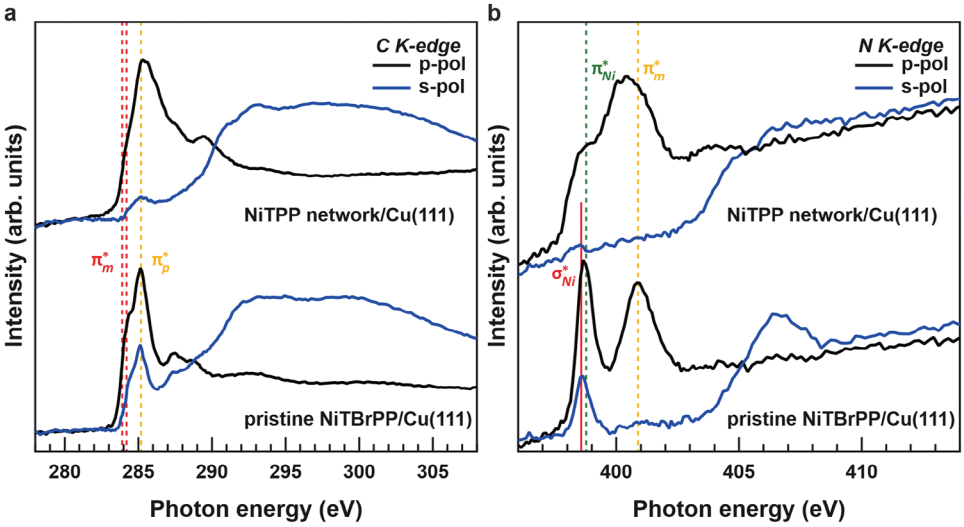

Figure 3. NEXAFS spectra recorded across both the a) C and b) N K-edges for 0.7 ML pristine NiTBrPP and the NiTPP-based network, obtained by annealing, on Cu(111).

dichroism for the as-deposited NiTBrPP on Cu(111), which indicates a significant tilt off the surface of the phenyl rings and a partial distortion or rehybridization of the macrocycle. This could be related to the strong interaction of the unsaturated phenyl groups with the surface that is driven by the flexibility of the activated NiTPP radicals. For comparison, the macrocycle of NiTPP deposited on the more reactive Cu(100) surface is mostly planar and parallel to the surface.[18,21,28–30] The linear dichroism is drastically enhanced after annealing the molecular layer to 473 K and inducing the intermolecular coupling. From the observed changes in the C K-edge spectrum, the formation of a 2D covalent NiTPP-based network is clearly evident. The π*-resonances are broadened and nearly vanish when using s-polarized light. This is characteristic of the formation of a π-extended covalent nanostructure with flat phenyl substituents, which are closely parallel to the surface plane due to cyclo-dehydrogenation side reactions.[8,31]

A better understanding of the interaction of the macrocycle with the surface can be obtained from the N K-edge spectra. The resonances observed in the N K-edge spectra of metalloporphyrins can be classified into pure macrocycle (index m) states and states arising from the mixing of metal 3d and N ligand 2p states (index Ni).[25,26,28] The low energy region is characterized by a π*-resonance sensitive to the Ni $3d_{xz,yz}$ to N ligand p_z backbonding that is strongly pronounced for the pristine molecular layer when using p-polarized light.

The strong signal in the low energy region for as-deposited NiTBrPP in s-polarization cannot be simply attributed to the characteristic Ni-to-N backbonding resonance since the main position is shifted to slightly lower photon energies. Indeed, a σ*-resonance associated with the direct N $2p_{x,y}$ to Ni $3d_{x^2-y^2}$ bonding is known to be strongly pronounced for a weak molecule-substrate interaction when using s-polarized light.[28] Overall, the close energy overlap of the first π*- and σ*-resonances at a photon energy of ≈398.7 eV prevents a clear estimate of the linear dichroism. The resonance at a higher photon energy of ≈400.9 eV corresponds to pure π*-symmetry resonances localized on the pyrroles and the perfect linear dichroism (no intensity in s-polarization) indicates a closely planar macrocycle, parallel to the surface. Hence, the residual intensity in s-polarization observed at the C K-edge for the macrocycle might be attributed to the rehybridization of the corresponding MO rather than to a geometric/conformational effect. The Ni(II) to Ni(I) reduction upon formation of the covalent NiTPP-based network after annealing to 473 K is due to an increase in the molecule-substrate interaction, as the phenyl constituents are also forced into a flat configuration. Indeed, this is reflected even in the N K-edge spectra. The resonances corresponding to the Ni—N interaction are quenched upon polymerization as a consequence of the more pronounced charge transfer at the interface.[28] At the same time, all resonances are shifted toward lower photon energies.[32] We further remark on the broadening of the pure macrocycle π*-resonance, which reflects the formation of a covalent nanomesh with an extended degree of π-conjugation.[8,31] NiTPP units within polymerized nanomeshes are known to be dehydrogenated on Au(111).[8,31] Even though the intermolecular coupling occurred at the predefined connection points defined by the Br positions in the NiTBrPP precursor, a control on the different dehydrogenation pathways was not observed. Consequently, the local structure of the covalent NiTPP network varied across the supporting surface. The situation on Cu(111) is presumably similar as the different pathways of these dehydrogenation reactions were also observed for various porphyrins on this substrate.[33,34] It was, however, shown that different porphyrin dehydrogenation pathways result in similar spectroscopic and magnetic properties.[8,9] The usage of ensemble techniques to probe the properties of molecules appears reasonable here to gather information about the magnetic properties of the functional Ni centers embedded into the molecular network. To characterize the magnetic properties of the Ni centers within the molecular network, we conducted XMCD experiments. For one-dimensional porphyrin chains, it was shown that the magnetic properties of the functional transition metal centers are identical to their single-molecule counterparts.[9] To understand the effect that the embedding of Ni centers into a 2D π-extended structure has on the magnetic properties, a comparison with a proper single-molecule reference appears necessary. Since the as-deposited NiTBrPP units are characterized by the Ni(II) oxidation state, we stabilized NiTPP units that were cyclo-dehydrogenated and, thus, flattened (dh-NiTPP) on Cu(111). For this monomer reference layer, the Ni ion is also reduced to the Ni(I) oxidation state. The details are further elaborated in Section S1 (Supporting Information), which summarizes all experimental details. Shortly, the deposition of NiTPP at low deposition rates on the hot Cu(111) surface held at 500 K allows us to obtain high coverages (we estimated the ML of dh-NiTPP) of fully dehydrogenated flat molecules as a single-molecule reference. It was found for NiTPP on Cu(100) that the strong molecule-substrate interaction results in high thermal stability of the molecular layer pinned to the surface.[29]

Therefore, a procedure allowing for the direct thermal activation of the molecules before they form a stable self-assembled layer was realized to fully dehydrogenate the molecular layer. The XMCD signals obtained by subtraction of the absorption spectrum collected with the light of positive helicity (σ^+) from the one collected with the light of negative helicity (σ^-) at the Ni $L_{3,2}$-edge for the dh-NiTPP layer and NiTPP network (obtained by annealing 0.5 ML of NiTBrPP to 473 K) are depicted in **Figure 4**. A magnetic field B of 6.8 T was used to ensure saturation conditions as is further elaborated when discussing the magnetization curves that the different systems exhibit. For this definition the dichroic signal at the L_3-edge is negative. Measurement geometries at photon incidence angles of $\theta = 0°$ (normal, left) and $\theta = 70$ (grazing, right) with respect to the surface normal were realized by rotating the sample to keep the photon propagation direction along the applied magnetic field. The spectra characteristics of the NiTPP network were multiplied to get the same XMCD magnitude at the L_2 edge to account for the lower signals due to the lower coverage necessary for the preparation. It has to be noted that the signals obtained at normal incidence are characterized by generally higher intensity, as is evident from the overview of their integrals presented in Figure S1 (Supporting Information) of the SI. Data obtained in grazing incidence is shown in similar magnitude here to enhance the clarity of the observed effects. The collected XMCD signals are similar when it comes to the energy position where the maximum effect (≈852.7 eV) is observed. Indeed, the spectral shape is very similar to the ones observed for paramagnetic transition metal ion $3d^9$ configurations.[30,35,36]

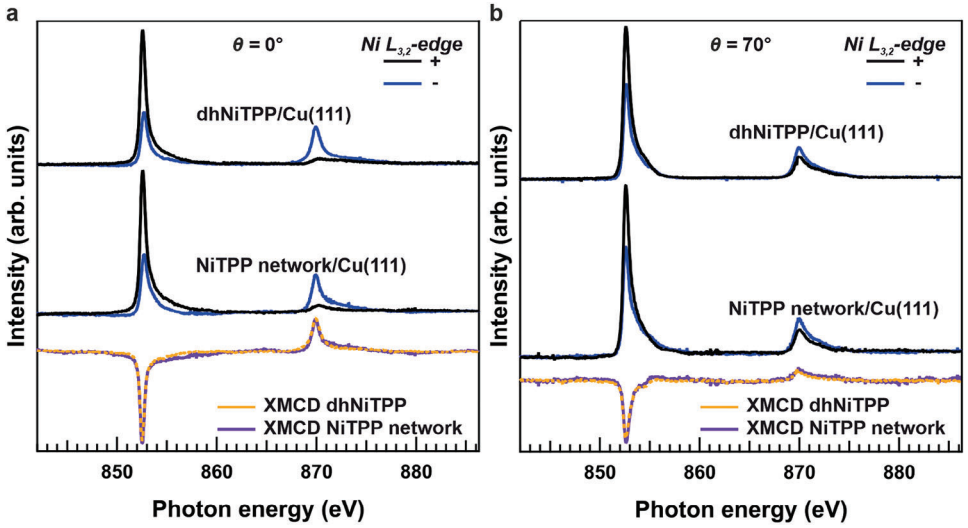

Figure 4. XMCD signals obtained across the Ni $L_{3,2}$-edge (B = 6.8 T along the photon incidence axis) for both dh-NiTPP and NiTPP network on Cu(111) at an incidence angle of: a) $\theta = 0$ and b) $\theta = 70$. All spectra of the NiTPP network were multiplied to get the same XMCD magnitude at the L_2-edge as for the dh-NiTPP layer.

This is fitting well with a Ni(II) to Ni(I) reduction at the reactive Cu(111) interface when compared to the molecular gas phase properties. Though they are also similar in shape, the XMCD signals in Figure 4 for both geometries indicate differences in the orbital momentum configurations characteristic of the Ni(I) centers of the dh-NiTPP single-molecule reference and NiTPP-based covalent networks. To further elaborate on this, a sum rule analysis was performed assuming one hole for the singly unoccupied Ni $3d_{x^2-y^2}$-based MO.[37,38] The deduced orbital and effective spin magnetic moments in the respective geometries for the different systems are summarized in **Table 1**.

The background-subtracted $\sigma^+ + \sigma^-$ absorption spectra displayed in Figure S1 (Supporting Information) were integrated and used to calculate the isotropic absorption intensity as specified in Section S2 (Supporting Information). Stepanow et al. found a $(\cos^2(\theta)+1)/2$ dependence of the $\sigma^+ + \sigma^-$ spectral intensity and accounted for this when calculating the isotropic absorption intensity.[36] We did not observe the same trend when looking at the intensity of the integrated absorption spectra. However, for both dh-NiTPP molecules and NiTPP-based networks the $\sigma^+ + \sigma^-$ intensity is similarly reduced in the range of ≈30% as evident from the spectra depicted in Figure S2 (Supporting Information). Therefore, errors coming from assumptions on the isotropic absorption intensity lead to wrong absolute results when doing the sum rule analysis. Yet, the relative trend can be considered well-displayed due to the similarities in the angular trend for the absorption intensities of both systems. Note that the errors given for the calculated momenta were further obtained by varying the subtracted background and the integral ranges in the sum rule analysis by a few eV to account for spectral noise. Furthermore, it has to be emphasized that the Ni centers characteristic of the dh-NiTPP single-molecule reference and NiTPP-based covalent networks on Cu(111) could vary slightly in their oxidation state, as the coinciding XMCD maxima positions might not necessarily imply an identical electronic configuration. Again, the angular dependence of the $\sigma^+ + \sigma^-$ spectra intensity that is practically identical has to be highlighted. Therefore, slight variations in the oxidation state would not affect the relative trend, but just the absolute values of the magnetic momenta calculated.

Table 1. Effective spin $m_{S,\,eff.}$ and orbital m_L magnetic moments obtained by sum rule analysis from different measurement geometries at $B = 6.8$ T for both dh-NiTPP and NiTPP network on Cu(111).

System		$\theta = 0°$	$\theta = 70°$
dh-NiTPP	$m_{S,\,eff}\,/\mu_B$	1.36 ± 0.36	0.50 ± 0.13
	$m_L\,/\mu_B$	0.10 ± 0.03	0.12 ± 0.03
NiTPP network	$m_{S,\,eff}\,/\mu_B$	1.40 ± 0.37	0.45 ± 0.11
	$m_L\,/\mu_B$	0.24 ± 0.05	0.05 ± 0.02

When comparing the two systems, it is evident that the formation of the π-extended NiTPP network results in an enhancement of the out-of-plane orbital momentum, while the in-plane orbital momentum is quenched with respect to the single-molecule reference. The spin magnetic moment behaves similarly for both systems. An angle-dependent deviation from the spin magnetic moment expected for a Ni $3d^9$ configuration with one unpaired electron can be attributed to the intra-atomic magnetic dipole moment.[39] However, the anisotropy of the spin magnetic moment is very similar for both the NiTPP networks and dh-NiTPP.[5] This, again, confirms the conclusion based on the XMCD maxima position that the strong charge transfer at the interface leads to similar Ni(I) species in both cases and that relative trends based on our comparative approach are well-displayed.

In contrast to what would be expected for similar magnetic Ni centers, the magnetization curves of both systems significantly differ as evident from **Figure 5**. We observed no differences between the magnetization curves at normal and grazing incidence for both systems. Therefore, the magnetization curves of both dh-NiTPP and NiTPP network on Cu(111) were used to fit the molecular spin S by using Brillouin functions with a g-factor of 2 that

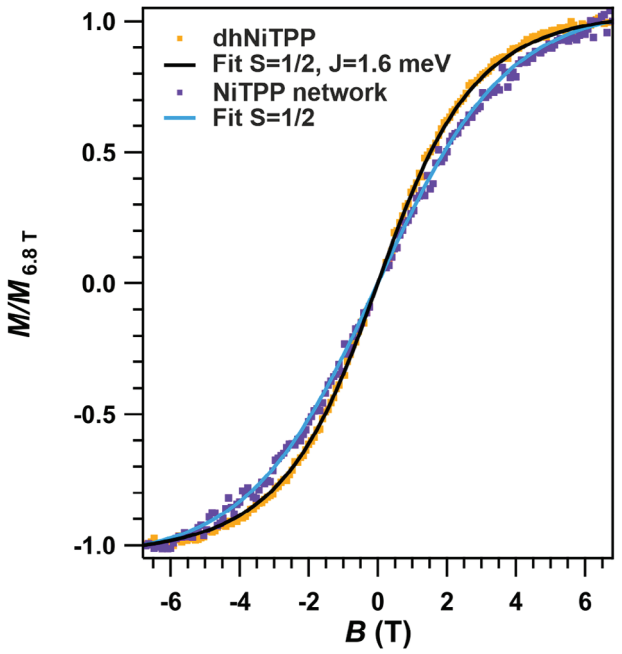

Figure 5. Magnetization curves acquired for both dh-NiTPP and NiTPP network on Cu(111) at $\theta = 0$ along with the corresponding fits for a $S = 1/2$ paramagnetic (Brillouin function) response and $S = 1/2$ subject to a mean-field (energy width of the itinerant spin density $W = 0.1$ eV and exchange coupling constant $J = 1.6$ meV). For both fits a temperature of 2.5 K and a *g*-factor of 2 were used.

account for a spin-only paramagnetic response at 2.5 K. The magnetization M was normalized to 1 at $B = 6.8$ T for all curves. For the NiTPP-based network, the $S = 1/2$ Brillouin function (cyan curve) reproduces the magnetic response, which agrees well with the XMCD findings. In contrast, dh-NiTPP on Cu(111) apparently exhibits an $S = 1$ behavior (not shown). We note that the sum rule error does not justify this discrepancy. More importantly, $S = 1$ would correspond to a $3d^8$ Ni center in a high-spin configuration for which a different shape of the absorption spectra to the experimental one is expected, as a consequence of an additional 3d hole.[30,40,41] Therefore, we expect a similar Ni $3d^9$ configuration for both the NiTPP network, which exhibits the expected $S = 1/2$ behavior, and the dh-NiTPP, whose magnetic response appears to be ferromagnetically enhanced.

We note that Ruderman–Kittel–Kasuya–Yosida (RKKY) exchange interaction mediated by substrate electrons was observed for similar molecular layers.[42] For ZnTPP units modified via cyclo-dehydrogenation, a preferential on-surface orientation was found.[43] This leads to preferential intermolecular arrangements, even though there is no long-range order in the molecular layer. A rough estimate of the published data allows us to identify a quite narrow window of 1.5–1.7 nm as the distance between the Zn centers, which we assume representative of dh-NiTPP units. The same statement applies to the polymerized NiTPP network, for which a similar distance window between the transition metal centers can be estimated.[8] Hence, even with the assumption of well-defined RKKY interactions in unordered molecular layers, different magnetic responses of the two systems as a consequence of pronounced variations in the Ni center distances are unlikely. Furthermore, the Ni center distance is in the range where the RKKY exchange interaction is expected to be rather weak on Cu(111).[44–46]

A close inspection of the NEXAFS spectra recorded across the N K-edge of both systems, which are displayed in Figure S2 (Supporting Information), indicates that the interaction of the macrocycle of dh-NiTPP with the supporting substrate is stronger than in the case of NiTPP network. This stronger interaction, which we attribute to a shorter molecule-substrate distance characteristic of the dh-NiTPP layer when compared to the polymerized NiTPP-based structure, may explain a significant difference in the amount of charge transferred to the molecular macrocycle. For the dh-NiTPP layer on Cu(111), this may result in a ferromagnetic interplay between the Ni 3d-based MOs and macrocycle-based MOs.[47] To obtain an estimate of the magnitude of the exchange coupling constant J, we performed a fitting of the magnetization curve characteristic of dh-NiTPP on Cu(111) using a mean-field-like approach reported in the literature. Thereby, the coordinated Ni ions with an $S = 1/2$ in a quadratic planar coordination environment were assumed to be influenced by four neighbors. The equations, which couple the molecular spin and the mean-field itinerant spin density to describe the magnetization of the system, were reported by Faraggi et al. and include J as a fitting parameter depending on the energy width W of the itinerant spin density.[48] For $W = 0.1$ eV, we obtained an exchange coupling constant $J = 1.6$ meV upon fitting of the experimental magnetization curve characteristic of dh-NiTPP on Cu(111). The corresponding fit (black curve) is further included in Figure 5. Again, a *g*-factor of 2 was used. For additional values of $W = 0.5$ and 0.7 eV, fits as good as the one presented in Figure 5 were obtained for exchange coupling constants $J = 3.9$ and 4.6 meV, respectively. Applying the mean-field approximation gives an estimate of the order of magnitude of the exchange coupling constant J, which agrees with that reported for similar systems.[47]

Additionally, from our theoretical model, based on the molecular cluster approach already validated to transition metal (Fe, Co, and Ni)TPP,[49–53] we find that the Ni—Cu distance can be varied in a certain range for which the Ni(II) to Ni(I) reduction is observed. The details are elaborated in Section S1 (Supporting Information). As our gas phase calculations revealed that the spiral dehydrogenated form is the most stable one,[53] we limited our attention to this NiTPP derivative to understand the implications of on-surface polymerization. Upon Ullmann polymerization at the interface, the structures are formed in the kinetic limit so that there is a random relation between the supporting substrate when it comes to the adsorption site and azimuthal orientation.[31] It was shown for similar Ullmann coupling phenomena on the Au(111) and Ag(111) surfaces that the Ni centers stabilized in the polymeric nanomeshes are still characterized by a uniform character.[8] An equivalent small influence of the random distribution of Ni centers on the Cu(111) surface is also supported by the similarity in the energy of different NiTPP units on the various adsorption sites of the Cu(111) surface.[54] A simplified theoretical model of the network formed via Ullmann coupling is based on a tetramer constituted by covalently connected spiral dh-NiTPP units. The molecular cluster approach is used to simulate the Cu-Ni interaction to account for the central Ni ion reduction at the interface with respect to the gas phase Ni(II).[53] A Ni—Cu distance of 2.1 Å was obtained from periodic

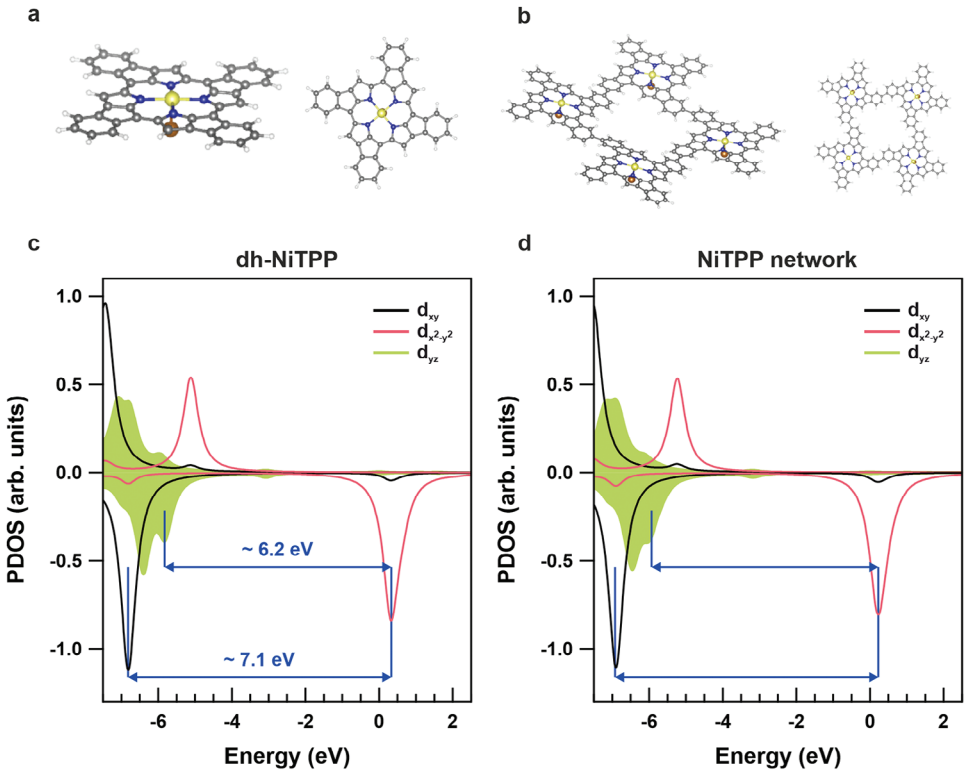

Figure 6. Side and top views of the structures obtained within the molecular cluster approach for supported a) dh-NiTPP ($C_{44}H_{20}N_4Ni$) and b) truncated NiTPP network ($[C_{44}H_{16}N_4Ni]_4$). Ni 3d-based PDOS (250 meV widths) calculated for both stabilized c) dh-NiTPP and d) truncated NiTPP network with positive (negative) values corresponding to spin up (down) electrons.

calculations for similar systems where the central Ni centers of porphyrin were experiencing similar charge transfer and consequently reduced to Ni(I) on Cu(100). In our model, we observe the Ni(II) to Ni(I) reduction already at distances of 2.2 Å. Therefore, we conclude that there exists a distance window for which the Ni(II) to Ni(I) reduction at the interface might appear. This is strongly supported by our experimental data that suggests a difference in the Ni—Cu distance for both systems, for which the Ni oxidation state is quite similar (see Section S3 Supporting Information). To obtain information sensitive to the effects induced by polymerization on the Ni 3d-based MOs, we assumed the same Ni-Cu distance (2.1 Å) for the supported dh-NiTPP and truncated NiTPP network. Top and side views of the obtained structures for the supported dh-NiTPP and NiTPP-based truncated network are displayed in **Figure** 6a,b. For both systems, the molecular constituents remain in a flat configuration after including the reduction of the Ni centers due to the interaction with the substrate in accordance with the experimental findings discussed above. When considering identical Ni-Cu distances for both dh-NiTPP and a patch of NiTPP network as a case study for the difference in the Ni centers of the two systems, we find the same relative energy level alignment for the Ni 3d-based MOs as further evident from Figure 6c,d, which display the Ni partial density of states (PDOS) for selected Ni 3d-based MOs for both the spin-up (positive) and spin-down (negative) channels. The presented 3D-based MOs are the ones relevant for the orbital magnetic moment of the coordinated Ni centers. The Fermi levels are at ≈ −5 eV. In both cases, the partially unoccupied MOs are the spin-down Ni $3d_{x^2-y^2}$-based ones, in agreement with a $3d^9$ configuration suggested by the experimental findings. The energy differences between the Ni $3d_{x^2-y^2}$-based and Ni $3d_{xy}/3d_{yz}$-based MOs characteristic of dh-NiTPP in the spin-down channel are indicated by blue arrows with the numeric values indicated. These energy differences are further included in the Ni PDOS characteristic of a simplified covalent NiTPP-based network. The right ends of the arrows are shifted to the maximum of the spin-down Ni $3d_{x^2-y^2}$-based MO for better comparison, which is stabilized ≈at 0.1 eV when comparing the supported NiTPP polymer with dh-NiTPP. We note that the relative energy-level alignment of the Ni 3d-based MOs is not changed for the two systems, which allows concluding that the effects induced by polymerization are not the origin of the change in the orbital magnetic moment anisotropy. The most relevant variation between the dh-NiTPP and NiTPP network is that the out-of-plane MOs of the polymerized structure are characterized by pronounced delocalization effects (see Section S3, Supporting Information). As such, the formation of the more rigid π-extended structure allows to influence of the interaction with the substrate and the thereby observed increase in the orbital momentum anisotropy is known to be beneficial to the increase of the magnetic anisotropy.[55] It was shown for d^9 systems where the functional transition metal ion is embedded in a similar environment that the orbital momentum anisotropy can be rationalized in terms of spin-orbit coupling effects.[36] The orbital angular momentum of the crystal field states is restored for the transition metal ion as excited states can admix differently depending on the orientation of the paramagnetic complex in a

magnetic field. Indeed, the thereby induced orbital momentum was shown to increase for decreasing energy differences between the Ni $3d_{x^2-y^2}$-based MO and the Ni $3d_{xy}$-(out-of-plane) or the Ni $3d_{xz,yz}$-based MOs (in-plane).[36] For the two systems presented here, the Ni-Cu distance is subject to variation and increased for the more rigid NiTPP network, which corresponds to an effective axial elongation of the square pyramidal ligand field upon polymerization of NiTPP units. The relative energy-level alignment of the 3D-based MOs is expected to be altered in accordance with the changes necessary for rendering an enhanced orbital magnetic moment anisotropy of Ni centers characteristic of the NiTPP-based network.[56]

3. Conclusion

We studied the formation of covalent NiTPP-based 2D networks that were created by Ullmann coupling on Cu(111). At the reactive interface, the functional Ni centers embedded into the polymeric nanomesh are distinct from their gas phase Ni(II) configuration as they are reduced to Ni(I) as a consequence of charge transfer from the substrate. This activates molecular magnetism at the interface since the Ni centers are characterized by an unpaired electron. To elucidate the consequences of the formation of a polymerized fully π-extended molecular porphyrin backbone, we compared the NiTPP-based network to a proper single-molecule reference, i.e., dh-NiTPP obtained by the dehydrogenation and flattening of NiTPP. Based on NEXAFS and XMCD, we were able to characterize the chemical differences and implications on the functional Ni centers when embedded into an π-extended molecular network. The rigidity in the molecular layer introduced by on-surface polymerization allows frontier electronic structure tuning, as expressed by the observed changes in the magnetic properties of the Ni centers. We emphasize the multifunctionality of the device, whose molecular backbone allows the engineering of the molecule-substrate interaction. The findings presented here are relevant in the design of more robust covalent materials with improved optoelectronic properties aimed at sophisticated applications like single-ion catalysis, sensors as well as molecular spintronics. The structural adaptions caused by interconnecting molecular units further introduce a pathway for regulating the properties of coordinated transition metal centers.

Supporting Information

Supporting Information is available from the Wiley Online Library or from the author.

Acknowledgements

The authors thank for access to the Swiss Light Source and Elettra Synchrotron. Part of the data shown was obtained at the ALOISA beamline through funding from the European Union's Horizon 2020 research and innovation program under grant agreement No 101007417, having benefitted from the access provided by CNR-IOM in Trieste within the framework of the NFFA-Europe Pilot Transnational Access Activity, proposal ID179 and ID400. D.B. and V.F. thank Dr. A. Barla for the fruitful discussion.

Open access funding enabled and organized by Projekt DEAL.

Conflict of Interest

The authors declare no conflict of interest.

Data Availability Statement

The data that support the findings of this study are available from the corresponding author upon reasonable request.

Keywords

magnetic properties, photoelectron spectroscopy, porphyrinoids, surface chemistry, X-ray absorption spectroscopy

Received: February 9, 2024
Revised: April 19, 2024
Published online: May 2, 2024

[1] W. Auwärter, D. Écija, F. Klappenberger, J. V. Barth, *Nat. Chem.* **2015**, *7*, 105.
[2] J. M. Gottfried, *Surf. Sci. Rep.* **2015**, *70*, 259.
[3] P. Knecht, P. T. P. Ryan, D. A. Duncan, L. Jiang, J. Reichert, P. S. Deimel, F. Haag, J. T. Küchle, F. Allegretti, T.-L. Lee, M. Schwarz, M. Garnica, W. Auwärter, A. P. Seitsonen, J. V. Barth, A. C. Papageorgiou, *J. Phys. Chem. C* **2021**, *125*, 3215.
[4] P. Knecht, J. Reichert, P. S. Deimel, P. Feulner, F. Haag, F. Allegretti, M. Garnica, M. Schwarz, W. Auwärter, P. T. P. Ryan, T. Lee, D. A. Duncan, A. P. Seitsonen, J. V. Barth, A. C. Papageorgiou, *Angew. Chem., Int. Ed.* **2021**, *60*, 16561.
[5] L. M. Arruda, M.d. E. Ali, M. Bernien, F. Nickel, J. Kopprasch, C. Czekelius, P. M. Oppeneer, W. Kuch, *J. Phys. Chem. C* **2019**, *123*, 14547.
[6] L. Grill, S. Hecht, *Nat. Chem.* **2020**, *12*, 115.
[7] L. Grill, M. Dyer, L. Lafferentz, M. Persson, M. V. Peters, S. Hecht, *Nat. Nanotechnol.* **2007**, *2*, 687.
[8] D. Baranowski, I. Cojocariu, A. Sala, C. Africh, G. Comelli, L. Schio, M. Tormen, L. Floreano, V. Feyer, C. M. Schneider, *Angew. Chem., Int. Ed.* **2022**, 61, 202210326.
[9] B. Mallada, P. Błoński, R. Langer, P. Jelínek, M. Otyepka, B. de la Torre, *ACS Appl. Mater. Interfaces* **2021**, *13*, 32393.
[10] M. Lackinger, *Chem. Commun.* **2017**, *53*, 7872.
[11] T. Wölfle, A. Görling, W. Hieringer, *Phys. Chem. Chem. Phys.* **2008**, *10*, 5739.
[12] P. Donovan, A. Robin, M. S. Dyer, M. Persson, R. Raval, *Chem. –Eur. J.* **2010**, *16*, 11641.
[13] G. Di Santo, S. Blankenburg, C. Castellarin-Cudia, M. Fanetti, P. Borghetti, L. Sangaletti, L. Floreano, A. Verdini, E. Magnano, F. Bondino, C. A. Pignedoli, M.-T. Nguyen, R. Gaspari, D. Passerone, A. Goldoni, *Chem. –Eur. J.* **2011**, *17*, 14354.
[14] T. A. Pham, F. Song, M.-T. Nguyen, Z. Li, F. Studener, M. Stöhr, *Chem. –Eur. J.* **2016**, *22*, 5937.
[15] M. Chen, J. Xiao, H.-P. Steinrück, S. Wang, W. Wang, N. Lin, W. Hieringer, J. M. Gottfried, *J. Phys. Chem. C* **2014**, *118*, 6820.
[16] G. Galeotti, M. Di Giovannantonio, J. Lipton-Duffin, M. Ebrahimi, S. Tebi, A. Verdini, L. Floreano, Y. Fagot-Revurat, D. F. Perepichka, F. Rosei, G. Contini, *Faraday Discuss.* **2017**, *204*, 453.
[17] R. Gutzler, L. Cardenas, J. Lipton-Duffin, M. el Garah, L. E. Dinca, C. E. Szakacs, C. Fu, M. Gallagher, M. Vondráček, M. Rybachuk, D. F. Perepichka, F. Rosei, *Nanoscale* **2014**, *6*, 2660.
[18] G. Zamborlini, M. Jugovac, A. Cossaro, A. Verdini, L. Floreano, D. Lüftner, P. Puschnig, V. Feyer, C. M. Schneider, *Chem. Commun.* **2018**, *54*, 13423.

[19] M. di Giovannantonio, M. el Garah, J. Lipton-Duffin, V. Meunier, L. Cardenas, Y. Fagot Revurat, A. Cossaro, A. Verdini, D. F. Perepichka, F. Rosei, G. Contini, *ACS Nano* **2013**, *7*, 8190.
[20] Q. Fan, T. Wang, L. Liu, J. Zhao, J. Zhu, J. M. Gottfried, *J. Chem. Phys.* **2015**, *142*, 101906.
[21] G. Zamborlini, D. Lüftner, Z. Feng, B. Kollmann, P. Puschnig, C. Dri, M. Panighel, G. Di Santo, A. Goldoni, G. Comelli, M. Jugovac, V. Feyer, C. M. Schneider, *Nat. Commun.* **2017**, *8*, 335.
[22] J. Stöhr, D. A. Outka, *Phys. Rev. B* **1987**, *36*, 7891.
[23] M. Chen, X. Feng, L. Zhang, H. Ju, Q. Xu, J. Zhu, J. M. Gottfried, K. Ibrahim, H. Qian, J. Wang, *J. Phys. Chem. C* **2010**, *114*, 9908.
[24] N. Schmidt, R. Fink, W. Hieringer, *J. Chem. Phys.* **2010**, *133*, 054703.
[25] S. A. Krasnikov, A. B. Preobrajenski, N. N. Sergeeva, M. M. Brzhezinskaya, M. A. Nesterov, A. A. Cafolla, M. O. Senge, A. S. Vinogradov, *Chem. Phys.* **2007**, *332*, 318.
[26] S. A. Krasnikov, N. N. Sergeeva, M. M. Brzhezinskaya, A. B. Preobrajenski, Y. N. Sergeeva, N. A. Vinogradov, A. A. Cafolla, M. O. Senge, A. S. Vinogradov, *J. Phys.: Condens. Matter* **2008**, *20*, 235207.
[27] C. C. Cudia, P. Vilmercati, R. Larciprete, C. Cepek, G. Zampieri, L. Sangaletti, S. Pagliara, A. Verdini, A. Cossaro, L. Floreano, A. Morgante, L. Petaccia, S. Lizzit, C. Battocchio, G. Polzonetti, A. Goldoni, *Surf. Sci.* **2006**, *600*, 4013.
[28] I. Cojocariu, H. M. Sturmeit, G. Zamborlini, A. Cossaro, A. Verdini, L. Floreano, E. D'Incecco, M. Stredansky, E. Vesselli, M. Jugovac, M. Cinchetti, V. Feyer, C. M. Schneider, *Appl. Surf. Sci.* **2020**, *504*, 144343.
[29] H. M. Sturmeit, I. Cojocariu, M. Jugovac, A. Cossaro, A. Verdini, L. Floreano, A. Sala, G. Comelli, S. Moro, M. Stredansky, M. Corva, E. Vesselli, P. Puschnig, C. M. Schneider, V. Feyer, G. Zamborlini, M. Cinchetti, *J. Mater. Chem. C* **2020**, *8*, 8876.
[30] H. M. Sturmeit, I. Cojocariu, A. Windischbacher, P. Puschnig, C. Piamonteze, M. Jugovac, A. Sala, C. Africh, G. Comelli, A. Cossaro, A. Verdini, L. Floreano, M. Stredansky, E. Vesselli, C. Hohner, M. Kettner, J. Libuda, C. M. Schneider, G. Zamborlini, M. Cinchetti, V. Feyer, *Small* **2021**, *17*, 2104779.
[31] S. A. Krasnikov, C. M. Doyle, N. N. Sergeeva, A. B. Preobrajenski, N. A. Vinogradov, Y. N. Sergeeva, A. A. Zakharov, M. O. Senge, A. A. Cafolla, *Nano Res.* **2011**, *4*, 376.
[32] A. Calabrese, L. Floreano, A. Verdini, C. Mariani, M. G. Betti, *Phys. Rev. B* **2009**, *79*, 115446.
[33] M. Röckert, M. Franke, Q. Tariq, S. Ditze, M. Stark, P. Uffinger, D. Wechsler, U. Singh, J. Xiao, H. Marbach, H.-P. Steinrück, O. Lytken, *Chem.–Eur. J.* **2014**, *20*, 8948.
[34] F. Xiang, A. Gemeinhardt, M. A. Schneider, *ACS Nano* **2018**, *12*, 1203.
[35] P. Gargiani, G. Rossi, R. Biagi, V. Corradini, M. Pedio, S. Fortuna, A. Calzolari, S. Fabris, J. C. Cezar, N. B. Brookes, M. G. Betti, *Phys. Rev. B* **2013**, *87*, 165407.
[36] S. Stepanow, A. Mugarza, G. Ceballos, P. Moras, J. C. Cezar, C. Carbone, P. Gambardella, *Phys. Rev. B* **2010**, *82*, 014405.
[37] B. T. Thole, P. Carra, F. Sette, G. van der Laan, *Phys. Rev. Lett.* **1992**, *68*, 1943.
[38] P. Carra, B. T. Thole, M. Altarelli, X. Wang, *Phys. Rev. Lett.* **1993**, *70*, 694.
[39] J. Stöhr, H. König, *Phys. Rev. Lett.* **1995**, *75*, 3748.
[40] I. Cojocariu, A. Windischbacher, D. Baranowski, M. Jugovac, R. C. de Campos Ferreira, J. Doležal, M. Švec, J. M. Zamalloa-Serrano, M. Tormen, L. Schio, L. Floreano, J. Dreiser, P. Puschnig, V. Feyer, C. M. Schneider, *Adv. Sci.* **2023**, *10*, 202300223.
[41] A. Köbke, F. Gutzeit, F. Röhricht, A. Schlimm, J. Grunwald, F. Tuczek, M. Studniarek, D. Longo, F. Choueikani, E. Otero, P. Ohresser, S. Rohlf, S. Johannsen, F. Diekmann, K. Rossnagel, A. Weismann, T. Jasper-Toennies, C. Näther, R. Herges, R. Berndt, M. Gruber, *Nat. Nanotechnol.* **2020**, *15*, 18.
[42] J. Girovsky, J. Nowakowski, M.d. E. Ali, M. Baljozovic, H. R. Rossmann, T. Nijs, E. A. Aeby, S. Nowakowska, D. Siewert, G. Srivastava, C. Wäckerlin, J. Dreiser, S. Decurtins, S.-X. Liu, P. M. Oppeneer, T. A. Jung, N. Ballav, *Nat. Commun.* **2017**, *8*, 15388.
[43] C. Ruggieri, S. Rangan, R. A. Bartynski, E. Galoppini, *J. Phys. Chem. C* **2016**, *120*, 7575.
[44] V. S. Stepanyuk, A. N. Baranov, D. V. Tsivlin, W. Hergert, P. Bruno, N. Knorr, M. A. Schneider, K. Kern, *Phys. Rev. B* **2003**, *68*, 205410.
[45] V. Stepanyuk, L. Niebergall, R. Longo, W. Hergert, P. Bruno, *Phys. Rev. B* **2004**, *70*, 075414.
[46] E. Simon, B. Újfalussy, B. Lazarovits, A. Szilva, L. Szunyogh, G. M. Stocks, *Phys. Rev. B* **2011**, *83*, 224416.
[47] Q. Sun, L. M. Mateo, R. Robles, P. Ruffieux, G. Bottari, T. Torres, R. Fasel, N. Lorente, *Adv. Sci.* **2022**, *9*, 2105906.
[48] M. N. Faraggi, V. N. Golovach, S. Stepanow, T.-C. Tseng, N. Abdurakhmanova, C. S. Kley, A. Langner, V. Sessi, K. Kern, A. Arnau, *J. Phys. Chem. C* **2015**, *119*, 547.
[49] I. Cojocariu, S. Carlotto, H. M. Sturmeit, G. Zamborlini, M. Cinchetti, A. Cossaro, A. Verdini, L. Floreano, M. Jugovac, P. Puschnig, C. Piamonteze, M. Casarin, V. Feyer, C. M. Schneider, *Chem.–Eur. J.* **2021**, *27*, 3526.
[50] I. Cojocariu, S. Carlotto, G. Zamborlini, M. Jugovac, L. Schio, L. Floreano, M. Casarin, V. Feyer, C. M. Schneider, *J. Mater. Chem. C* **2021**, *9*, 12559.
[51] S. Carlotto, I. Cojocariu, V. Feyer, L. Floreano, M. Casarin, *Nanomaterials* **2022**, *12*, 218.
[52] I. Cojocariu, S. Carlotto, D. Baranowski, M. Jugovac, L. Schio, L. Floreano, M. Casarin, V. Feyer, C. M. Schneider, *Inorg. Chim. Acta* **2023**, *556*, 121657.
[53] I. Cojocariu, S. Carlotto, D. Baranowski, M. Jugovac, J. Dreiser, L. Schio, L. Floreano, M. Casarin, V. Feyer, C. M. Schneider, *J. Mater. Chem. C* **2023**, *11*, 15521.
[54] S. Fatayer, R. G. A. Veiga, M. J. Prieto, E. Perim, R. Landers, R. H. Miwa, A. de Siervo, *Phys. Chem. Chem. Phys.* **2015**, *17*, 18344.
[55] P. Gambardella, S. Rusponi, M. Veronese, S. S. Dhesi, C. Grazioli, A. Dallmeyer, I. Cabria, R. Zeller, P. H. Dederichs, K. Kern, C. Carbone, H. Brune, *Science* **2003**, *300*, 1130.
[56] C. Zhao, X. Liu, J. Liu, J. Wang, X. Wan, C. Wang, X. Li, J. Shui, L. Song, H. Peng, B. Li, Q. Zhang, *Angew. Chem., Int. Ed.* **2023**, *62*, 202313028.